Classical and quantum responsivities of geometrically asymmetric metal-vacuum-metal junctions used for the rectification of infrared and optical radiations

A. Mayer[a)]
Laboratoire de Physique du Solide, University of Namur-FUNDP, Rue de Bruxelles 61, B-5000 Namur, Belgium

M. S. Chung
Department of Physics, University of Ulsan, Ulsan 680-749, Korea

P. B. Lerner
Quantum Transistor, LLC, Ithaca, New York 14850

B. L. Weiss
Department of Physics, 130 CAC, Pennsylvania State University, Altoona, Pennsylvania 16601

N. M. Miskovsky and P. H. Cutler
Department of Physics, 104 Davey Laboratory, Pennsylvania State University, University Park, Pennsylvania 16802

(Received 22 December 2010; accepted 21 May 2011; published 29 June 2011)

The authors study the rectification properties of geometrically asymmetric metal-vacuum-metal junctions in which a combination of static and oscillating biases is established between a cathode that is extended by a hemispherical protrusion and a flat anode. The static current-voltage characteristics of this device are established using a transfer-matrix methodology. The rectification properties of the device are, however, analyzed in the framework of a classical model that is based on the Taylor-expansion of static current-voltage data. This enables the impedance and the classical responsivity of the device to be established. The authors then investigate how the impedance and the classical responsivity of this junction are affected by the work function of the materials, the gap spacing between the cathode and the anode, and the aspect ratio of the protrusion. They also consider the efficiency with which the energy of incident radiations can be converted using this device. The authors finally compare the responsivity obtained using this classical approach with the quantum responsivity one can define from the currents actually achieved in an oscillating barrier. This work provides additional insight for the development of a device that could be used for the energy conversion of infrared and optical radiations. © *2011 American Vacuum Society.*
[DOI: 10.1116/1.3599756]

I. INTRODUCTION

Rectification and frequency-mixing of infrared radiations typically involve point-contact diodes that consist of metal-oxide-metal systems in which one of the metals is essentially flat while the other is extended by a sharp tip.[1–6] This rectification is essentially due to the geometrical asymmetry of these systems, although material and thermal asymmetry as well as the application of a static external bias can also contribute to this rectification.[7–11] Besides rectification and frequency-mixing, these systems were also used for the accurate measurement of infrared frequencies[12–14] and for applications as fundamental as the measurement of the speed of light[15,16] and the determination of tunneling times.[7,17,18] Current efforts aim at reducing their characteristic response times and at improving their responsivity.

The need for high-speed electronics and the challenge posed by the harvesting of solar energy renew the interest in these devices.[19,20] Rectification using these devices is indeed possible as long as electrons are able to cross the junction before the external field changes sign. Tunneling times are of the order of femtoseconds[18,21] so that the rectification of optical frequencies can in principle be achieved (the *RC* response time of the device must be sufficiently low to achieve an efficient biasing of the junction). Nanostructures are hence developed to collect the energy of electromagnetic radiations (with frequencies ranging from the near-infrared up to the visible),[22–24] while metal-insulator-metal or metal-vacuum-metal junctions are used for the rectification of these radiations.[25–30] Given the static current-voltage $I_{\mathrm{stat}}(V_{\mathrm{stat}})$ characteristics of these junctions, their ability to rectify oscillating signals is usually analyzed in terms of their classical responsivity $(d^2I_{\mathrm{stat}}/dV_{\mathrm{stat}}^2)/(dI_{\mathrm{stat}}/dV_{\mathrm{stat}})$. In conditions where quasistatic approximations apply, the rectified voltage as well as the quantum efficiency of the rectification are indeed proportional to this responsivity.[31,32] A record responsivity of 31 V^{-1} was reported by Choi *et al.*[30]

In previous work, we developed a transfer-matrix methodology for the modeling of metal-vacuum-metal junctions

[a)]Author to whom correspondence should be addressed; electronic mail: alexandre.mayer@fundp.ac.be

that are subject to an oscillating potential.[10,11,33,34] This quantum-mechanical scheme accounts for three-dimensional aspects of the problem as well as for the time-dependence of the barrier. In our first paper,[10] we analyzed the rectification properties of these junctions in the quasistatic approximation in which the angular frequency Ω of the external potential goes to zero ($\Omega \to 0$). Reference 11 is a generalization of this work that accounts for the time-dependence of the external potential explicitly ($\Omega \neq 0$). Electronic scattering in the junction is described within this formalism by the absorption or emission of energy quanta $\hbar\Omega$. In Ref. 33, we extended this formalism to enable the consideration of different models for the dielectric function of the materials present in the junction (this extension was required in order to study the effects of polarization resonances). These articles were relevant to the rectification of monochromatic radiations (given values of Ω). In Ref. 34, we finally extended this framework by studying the rectification of a full electromagnetic spectrum (field amplitudes representative of a focused beam of solar radiation). The results achieved using this methodology can be analyzed in terms of a classical theory that is based on the Taylor-expansion of the static $I_{stat}(V_{stat})$ characteristics. This enables the derivation of a "classical responsivity," which is the quantity addressed by other experimental/theoretical works for the characterization of similar devices.[25,28–30] This presentation of our results is therefore well suited for comparison. The impedance and the classical responsivity of the junction actually represent the quantities of interest for practical applications and we will seek at optimizing these quantities.

This article is organized according to the following lines. In Sec. II, we present the transfer-matrix methodology that is used for the quantum-mechanical derivation of current-voltage data. In Sec. III, we present the classical analysis technique that enables the derivation of quantities such as the classical responsivity for characterizing the response of the junction to an oscillating potential. In Sec. IV, we then present the impedance and classical responsivity of a nanometer-size tungsten junction. We will study how these quantities are affected by (i) a reduction of the work function, (ii) a modification of the gap spacing between the cathode and the anode, and (iii) a modification of the aspect ratio of the protrusion. We will also consider the efficiency with which the energy of an external radiation can be converted by this device. In Sec. V, we will finally investigate how the responsivities achieved using this classical approach compare with the effective responsivity one can define from the currents actually obtained in an oscillating barrier when the time-dependent scattering problem is solved exactly. This will provide useful insight for the development of a device that could be used for the energy conversion of infrared and optical radiations.

II. MODELING OF THE DIODE CURRENTS USING A TRANSFER-MATRIX METHODOLOGY

We assume that the junction consists of two perfect metals separated by a vacuum gap of length D. These metals are described by a Fermi energy E_F of 19.1 eV and a work function W of 4.5 eV (values for tungsten). The cathode in the region $z \leq 0$ and the anode in the region $z \geq D$ are also referred to as region I and region III, respectively. The intermediate gap region $0 \leq z \leq D$ is finally referred to as region II. We consider that the cathode supports a protrusion, which is part of region II. We assume in this whole work a room temperature T of 300 K.

We assume that the junction is subject to an external bias $V(t) = V_{stat} + V_{osc}\cos(\Omega t)$ that consists of a static component with amplitude V_{stat} and an oscillating component with amplitude V_{osc} and angular frequency Ω. By using the finite-difference techniques presented in Refs. 10, 34, and 35, one can compute the potential energy $V(\mathbf{r},t) = V_{stat}(\mathbf{r}) + V_{osc}(\mathbf{r})\cos(\Omega t)$ in the different parts of the system. $V_{stat}(\mathbf{r})$ accounts for the potential wells $-(E_F + W)$ associated with the metallic elements, for the image potentials in the vacuum,[36] and for the potentials induced by the static component of the external bias. $V_{osc}(\mathbf{r})\cos(\Omega t)$ describes the potentials induced by the oscillating component of the external bias (for materials whose dielectric function has a non-negligible imaginary component, one must use the more general expression provided in Ref. 34).

The currents that cross the junction are then obtained by solving the time-dependent Schrödinger equation $[-(\hbar^2/2m)\Delta + V(\mathbf{r},t)]\Psi(\mathbf{r},t) = i\hbar(\partial/\partial t)\Psi(\mathbf{r},t)$ with a Floquet expansion of the wave function.[37,38] The method consists in expanding the electronic wave function as $\Psi(\mathbf{r},t) = \sum_{k=-N}^{N} \Psi_k(\mathbf{r}) e^{-i(E+k\hbar\Omega)t/\hbar}$, where the different components of this expression account for the absorption/emission of energy quanta $\hbar\Omega$ and N is a cutoff parameter.[11] We then expand the $\Psi_k(\mathbf{r},t)$ in terms of basis states adapted to the use of cylindrical coordinates. We refer by $\Psi^{\mathrm{I},\pm}_{m,j,k}(\mathbf{r},t)$ and $\Psi^{\mathrm{III},\pm}_{m,j,k}(\mathbf{r},t)$ to the boundary states in regions I and III (m and j are the enumeration parameters, and the $\pm$ signs refer to the propagation direction relative to the z-axis).[10,11] By using the techniques developed in previous work,[10,11,39–42] we can then establish scattering solutions $\Psi^{+}_{m,j} \overset{z\leq 0}{=} \Psi^{\mathrm{I},+}_{m,j,0} + \sum_{m',j',k'} S^{-+}_{(m',j',k'),(m,j,0)} \Psi^{\mathrm{I},-}_{m',j',k'} \overset{z\geq D}{=} \sum_{m',j',k'} S^{++}_{(m',j',k'),(m,j,0)} \Psi^{\mathrm{III},+}_{m',j',k'}$ and $\Psi^{-}_{m,j} \overset{z\leq 0}{=} \sum_{m',j',k'} S^{--}_{(m',j',k'),(m,j,0)} \Psi^{\mathrm{I},-}_{m',j',k'} \overset{z\geq D}{=} \Psi^{\mathrm{III},-}_{m,j,0} + \sum_{m',j',k'} S^{+-}_{(m',j',k'),(m,j,0)} \Psi^{\mathrm{III},+}_{m',j',k'}$ that correspond to single incident states $\Psi^{\mathrm{I},+}_{m,j,0}(\mathbf{r})$ in region I and $\Psi^{\mathrm{III},-}_{m,j,0}(\mathbf{r})$ in region III. The integration of these scattering solutions finally provides the diode currents.[11]

III. CLASSICAL ANALYSIS OF STATIC CURRENT-VOLTAGE DATA

Let us assume that the currents I_{stat} actually induced by a *static* external bias V_{stat} have been established. The current $I(t)$ induced by a potential $V(t) = V_{stat} + V_{osc}\cos(\Omega t)$ may be obtained from the Taylor-expansion of these static data,[31,32] thus giving

$$I(t) = \sum_{n=0}^{\infty} \frac{1}{n!} \frac{d^n I_{\text{stat}}}{dV_{\text{stat}}^n} [V(t) - V_{\text{stat}}]^n. \quad (1)$$

This expression actually assumes that the diode currents follow instantaneously the external potential (limit where $\Omega \rightarrow 0$). This assumption will not hold when the period $T = 2\pi/\Omega$ of the external bias is comparable with the time taken by electrons to cross the junction, which is the case for optical frequencies. A limitation for practical applications is also given by the RC time constant of the device, which will reduce the effective biasing of the junction (very sharp tips are used in this context in order to reduce RC).[7] An exact calculation of the biasing $V(t)$ one would obtain with a complete device exceeds the scope of this article and we will merely assume that the components of $V(t)$ are given.

Using $V_{\text{osc}}^2 \cos^2(\Omega t) = V_{\text{osc}}^2/2[1+\cos(2\Omega t)]$ and similar trigonometric relations for the higher-order terms, one can actually express the diode current as $I(t) = \Sigma_{n=0}^{\infty} I_n \cos(n\Omega t)$, with $I_0 = I_{\text{stat}} + (V_{\text{osc}}^2/4)(d^2 I_{\text{stat}}/dV_{\text{stat}}^2) + (V_{\text{osc}}^4/64)(d^4 I_{\text{stat}}/dV_{\text{stat}}^4) + (V_{\text{osc}}^6/2304)(d^6 I_{\text{stat}}/dV_{\text{stat}}^6) + \ldots$, $I_1 = V_{\text{osc}}(dI_{\text{stat}}/dV_{\text{stat}}) + (V_{\text{osc}}^3/8)(d^3 I_{\text{stat}}/dV_{\text{stat}}^3) + (V_{\text{osc}}^5/192)(d^5 I_{\text{stat}}/dV_{\text{stat}}^5) + \ldots$, $I_2 = (V_{\text{osc}}^2/4)(d^2 I_{\text{stat}}/dV_{\text{stat}}^2) + (V_{\text{osc}}^4/48)(d^4 I_{\text{stat}}/dV_{\text{stat}}^4) + (V_{\text{osc}}^6/1536)(d^6 I_{\text{stat}}/dV_{\text{stat}}^6) + \ldots$, etc. The dc component of the diode current is thus given by

$$\langle I \rangle = I_{\text{stat}} + \frac{V_{\text{osc}}^2}{4} \frac{d^2 I_{\text{stat}}}{dV_{\text{stat}}^2} \quad (2)$$

if we keep only the lowest-order term in V_{osc}.

The energy gained, per unit of time, by the electrons that cross the junction is given by $\langle P \rangle = (\Omega/2\pi) \int_0^{2\pi/\Omega} V(t) I(t) dt = V_{\text{stat}} I_{\text{stat}} + V_{\text{osc}} I_1/2$. This classical expression only holds in the limit where the time taken by electrons to cross the junction is again significantly smaller than the period $2\pi/\Omega$ of the external potential.[11] Keeping only the lowest-order term in V_{osc}, we thus have

$$\langle P \rangle = V_{\text{stat}} I_{\text{stat}} + \frac{V_{\text{osc}}^2}{2} \frac{dI_{\text{stat}}}{dV_{\text{stat}}}. \quad (3)$$

The rectified bias V_{rect} corresponds to the static bias that would provide the same dc as $V_{\text{osc}} \cos(\Omega t)$. One can determine V_{rect} by the relation $V_{\text{rect}}(dI_{\text{stat}}/dV_{\text{stat}}) = \langle I \rangle - I_{\text{stat}}$. Using Eq. (2), we then obtain

$$V_{\text{rect}} = \frac{V_{\text{osc}}^2}{4} \frac{d^2 I_{\text{stat}}/dV_{\text{stat}}^2}{dI_{\text{stat}}/dV_{\text{stat}}}. \quad (4)$$

The quantum efficiency of the rectification process is defined in this context by $\eta_{\text{quant}} = [(\langle I \rangle - I_{\text{stat}})/(\langle P \rangle - V_{\text{stat}} I_{\text{stat}})]/[e/\hbar\Omega]$ in which the ratio between the dc induced by the oscillating potential $(\langle I \rangle - I_{\text{stat}})$ and the energy absorbed per unit of time by the electrons that cross the junction because of this oscillating potential $(\langle P \rangle - V_{\text{stat}} I_{\text{stat}})$ is compared with the quantum limit of $e/\hbar\Omega$. Using Eqs. (2) and (3), we obtain

$$\eta_{\text{quant}} = \frac{1}{2} \frac{\hbar\Omega}{e} \frac{d^2 I_{\text{stat}}/dV_{\text{stat}}^2}{dI_{\text{stat}}/dV_{\text{stat}}}. \quad (5)$$

The impedance $R = 1/(dI_{\text{stat}}/dV_{\text{stat}})$ and the classical responsivity $S = (d^2 I_{\text{stat}}/dV_{\text{stat}}^2/dI_{\text{stat}}/dV_{\text{stat}})$ thus represent the quantities of interest for characterizing the junction. Equation (2) is actually the classical limit of the quantum-mechanical result $\langle I \rangle = I_{\text{stat}} + (V_{\text{osc}}^2/4)(I_{\text{stat}}(V_{\text{stat}} + \hbar\Omega/e) - 2I_{\text{stat}}(V_{\text{stat}}) + I_{\text{stat}}(V_{\text{stat}} - \hbar\Omega/e)/(\hbar\Omega/e)^2)$ one obtains as special case of $\langle I \rangle = \Sigma_{n=-\infty}^{\infty} J_n^2(\alpha) I_{\text{stat}}(V_{\text{stat}} + n\hbar\Omega/e)$ when $\alpha = (V_{\text{osc}}/\hbar\Omega/e) \rightarrow 0$.[31,32] The J_n in this last expression are the Bessel functions. Equation (5) on the other hand only makes sense if $\eta_{\text{quant}} < 1$. The relations established in this section therefore require that $V_{\text{osc}} < (\hbar\Omega/e) < 2(d^2 I_{\text{stat}}/dV_{\text{stat}}^2/dI_{\text{stat}}/dV_{\text{stat}})^{-1}$. This analysis is hence useful for infrared frequencies. We will show in Sec. V that deviations appear when considering frequencies in the visible domain.

IV. CHARACTERIZATION OF A TUNGSTEN METAL-VACUUM-METAL JUNCTION

Experimental support for the rectification of optical radiations by geometrically asymmetric metal-vacuum-metal junctions is provided by the work of Nguyen *et al.*[18] In this experiment, a 1.06-μm yttrium-aluminum-garnet (YAG) laser was focused upon a scanning tunneling microscope (STM) junction consisting of a W-sharp tip and a polished flat Si(111) anode. The laser-induced dc current was measured as function of the tip-to-base spacing (starting from a tip-to-base spacing of 1 nm and considering higher values until the laser-induced current vanishes). The experiment revealed a cutoff distance of 2.5 nm. Assuming that the electrons cross the junction at the Fermi velocity, the analysis reveals that the transit time for a 1 nm gap is around 10^{-15} s, which corresponds to a radiation wavelength in the ultraviolet. The use of point-contact devices for the measurements of absolute frequencies up to the green part of the visible spectrum provides another experimental support to the rectification of optical frequencies.[43] Dagenais *et al.* experimentally verified that a geometrically asymmetric tunneling diode can be used for the rectification of radiations through the radio frequency region.[27] Bragas *et al.* used a 670 nm laser to irradiate a STM junction in order to determine the field enhancement as measured by optical rectification. Analysis of their data indicated optical rectification due to junction geometry as well as thermal asymmetry.[44] Ward *et al.* demonstrated both experimentally and theoretically that nonlinear tunneling conduction between gold electrodes separated by a subnanometer gap leads to optical rectification, producing a dc photocurrent when the gap is irradiated by a 785 nm laser source.[28] Although mechanical stability of earlier devices placed a limitation on the actual contact area, modern fabrication techniques have overcome the mechanical fragility of previous point-contact diodes and issues related to reproducible fabrication of nanoscale devices. The technological difficulty of producing arrays of nanometer gap junctions over areas of square-centimeters has recently been overcome by Gupta and Willis using atomic layer deposition (ALD).[45] Planar arrays of Cu-vacuum-Cu tunnel junctions were produced on silicon wafers using conventional lithography tech-

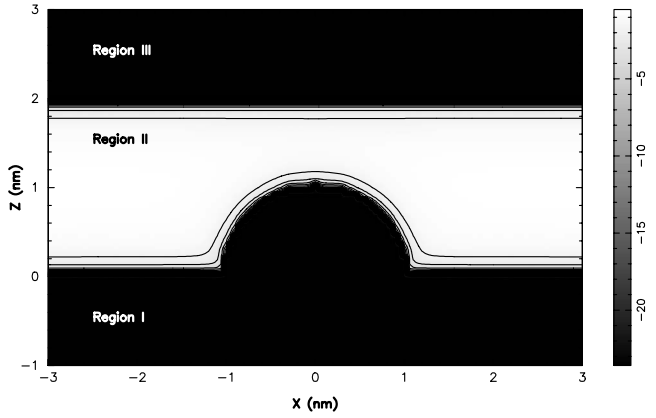

FIG. 1. Potential energy $V(\mathbf{r},t)$ in a metal-vacuum-metal junction. The representation corresponds to an external potential of 0 V. It includes the potential wells that characterize the metallic elements and the image potential in the vacuum. The height of the protrusion is 1 nm. The gap spacing D is 2 nm.

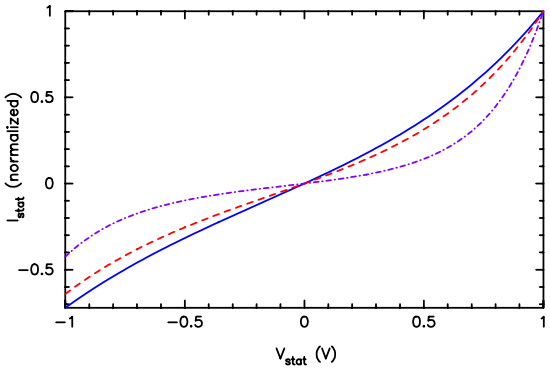

FIG. 2. (Color online) Static current-voltage data corresponding to work functions W of 4.5 eV (solid), 3 eV (dashed), and 1.5 eV (dot-dashed). The currents are normalized to values of 8.0×10^{-12} A for W=4.5 eV, 8.2×10^{-10} A for W=3 eV, and 1.2×10^{-6} A for W=1.5 eV. The height of the protrusion is 1 nm. The gap spacing D is 2 nm.

niques, followed by ALD to yield tunnel junctions of the order of 1 nm. These experiments reveal robustness against thermal expansion of the materials[28] and high vacuum does not appear to be a strict necessity.

We consider here an ideal metal-vacuum-metal junction made of tungsten. The system considered for the application of our transfer-matrix technique is actually restricted to a cylindrical region, whose radius R is 3 nm (this can be considered as the radius of two cylindrical plates that represent the cathode and the anode in our simulations).[10,11] The gap spacing D between the cathode and the anode is 2 nm. We finally consider that the cathode supports a hemispherical protrusion whose radius r is 1 nm (this protrusion is placed on the central z-axis of the system). This junction is represented in Fig. 1.

Using the transfer-matrix technique presented in Sec. II, we can establish the static current-voltage data of the diode. We hence considered a static potential V_{stat} ranging between -1 and $+1$ V and computed the corresponding diode currents I_{stat}. We take the convention that V_{stat} represents the electric potential of the anode minus the electric potential of the cathode. For $V_{\text{stat}}>0$, it is the cathode that emits electrons. The corresponding diode current I_{stat} is defined for convenience as positive. For $V_{\text{stat}}<0$, it is the anode that emits electrons and I_{stat} is negative by the same convention. The results achieved for the $I_{\text{stat}}(V_{\text{stat}})$ data are represented in Fig. 2.

Figure 2 clearly shows that the $I_{\text{stat}}(V_{\text{stat}})$ data are asymmetric with respect to the sign of V_{stat}. This asymmetry in the currents is of course related to the geometrical asymmetry of the junction. As explained in Sec. III, having an $I_{\text{stat}}(V_{\text{stat}})$ characteristics with $d^2I_{\text{stat}}/dV_{\text{stat}}^2\neq0$ is essential for achieving the rectification of oscillating signals. Even without the geometrical asymmetry, the condition $d^2I_{\text{stat}}/dV_{\text{stat}}^2\neq0$ can in general be reached by the application of a static bias V_{stat}. As shown later in this article, the external bias V_{stat} increases the classical responsivity S. On the other hand, it requires the user to provide an input power $V_{\text{stat}}I_{\text{stat}}$. For applications related to the energy conversion of incident radiations, this constitutes a loss that can only be tolerated in conditions where the power gained from the source of the oscillating barrier is larger (i.e., $(V_{\text{osc}}^2/2)(dI_{\text{stat}}/dV_{\text{stat}})>V_{\text{stat}}I_{\text{stat}}$). Figure 2 also includes the $I_{\text{stat}}(V_{\text{stat}})$ data achieved when the work function of both the cathode and the anode are reduced to 3 and 1.5 eV. A reduction of the work function can be achieved for example by coating the materials with caesium.[20,46] This reduction of the work function increases the asymmetry of the $I_{\text{stat}}(V_{\text{stat}})$ characteristics. It also increases the diode currents (maximal I_{stat} value of 8.0×10^{-12} A for W=4.5 eV, 8.2×10^{-10} A for W=3 eV, and 1.2×10^{-6} A for W=1.5 eV when considering a bias V_{stat} of 1 V).

We can then use the static $I_{\text{stat}}(V_{\text{stat}})$ data of Fig. 2 to compute the impedance $R=1/(dI_{\text{stat}}/dV_{\text{stat}})$ and the classical responsivity $S=\frac{d^2I_{\text{stat}}/dV_{\text{stat}}^2}{dI_{\text{stat}}/dV_{\text{stat}}}$ of the junction. This was done by (i) adjusting the three sets of data in Fig. 2 by ninth-order polynomial expressions and (ii) calculating analytically the derivatives of these expressions. The results achieved for the impedance and classical responsivity are represented in Fig. 3. The results correspond to a work function W of 4.5, 3, and 1.5 eV. The impedance R at zero bias is 2.0×10^{11} Ω for untreated tungsten (W=4.5 eV), 2.4×10^{9} Ω for W=3 eV, and 5.1×10^{6} Ω for W=1.5 eV. These impedances decrease for both signs of V_{stat}. The width of the tunneling barrier decreases indeed as soon as a voltage V_{stat} (either positive or negative) is applied through the junction. The decrease is, however, more significant for positive biases. Because of the hemispherical protrusion, the cathode is indeed a better field-emitter than the anode. Reducing the work function W finally reduces the impedance of the junction (this reduction indeed increases the field-emission currents). The value of $R=2.0\times10^{11}$ Ω for untreated tungsten is fully consistent with the value one can extract from the experimental data published by Dagenais *et al.* for a similar device (see Fig. 5 of their article).[27] In order to couple efficiently the diode to a nanoantenna, this diode impedance should however be as small as a few hundreds Ohms.[47] Reducing the work func-

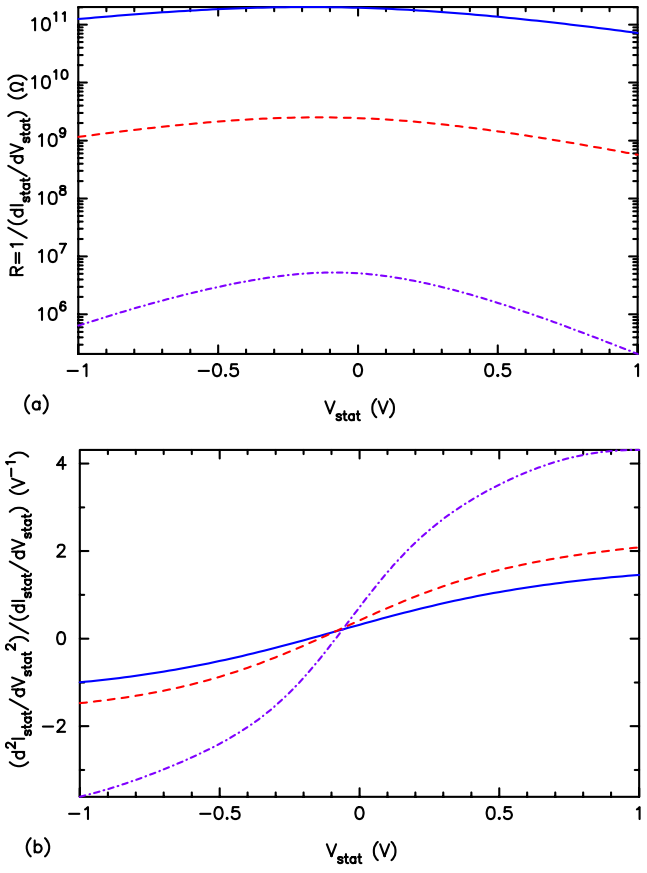

FIG. 3. (Color online) Impedance $R=1/(dI_{\text{stat}}/dV_{\text{stat}})$ (a) and classical responsivity $S=(d^2I_{\text{stat}}/dV_{\text{stat}}^2/dI_{\text{stat}}/dV_{\text{stat}})$ (b) corresponding to work functions W of 4.5 eV (solid), 3 eV (dashed), and 1.5 eV (dot-dashed). The height of the protrusion is 1 nm. The gap spacing D is 2 nm.

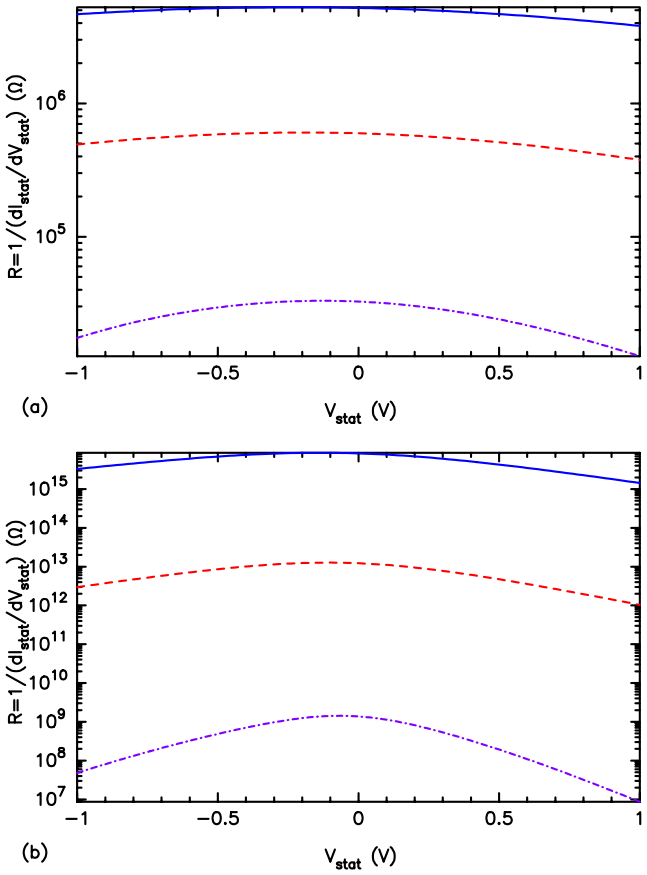

FIG. 4. (Color online) Impedance $R=1/(dI_{\text{stat}}/dV_{\text{stat}})$ of a diode with gap spacings D of 1.5 nm (a) and 2.5 nm (b). The work functions W are 4.5 eV (solid), 3 eV (dashed), and 1.5 eV (dot-dashed). The height of the protrusion is 1 nm.

tion appears to be a possibility to reach that objective. It will be shown that reducing the gap spacing D also reduces R.

The classical responsivity $S=(d^2I_{\text{stat}}/dV_{\text{stat}}^2/dI_{\text{stat}}/dV_{\text{stat}})$ of the diode varies smoothly between -1.0 and 1.5 V^{-1} for untreated tungsten ($W=4.5$ eV), between -1.5 V^{-1} and 2.1 V^{-1} for $W=3$ eV, and between -3.6 V^{-1} and 4.3 V^{-1} for $W=1.5$ eV. It appears therefore that reducing the work function of the materials has the combined advantage of (i) reducing the impedance R of the junction and (ii) increasing the classical responsivity S. This may be contrary to general expectation since the classical responsivity S is proportional to the impedance R $[S=R(d^2I_{\text{stat}}/dV_{\text{stat}}^2)$, with $R=1/(dI_{\text{stat}}/dV_{\text{stat}})]$. The variations of S result in reality from a trade-off between the variations of $dI_{\text{stat}}/dV_{\text{stat}}$ and those of $d^2I_{\text{stat}}/dV_{\text{stat}}^2$. For the conditions of this article (nanometer gap spacing D), both $dI_{\text{stat}}/dV_{\text{stat}}$ and $d^2I_{\text{stat}}/dV_{\text{stat}}^2$ present significant variations when reducing the work function W and the net effect is an increase of the classical responsivity S despite a reduction of the impedance R. The classical responsivity at zero bias is 0.32 V^{-1} for untreated tungsten ($W=4.5$ eV), 0.42 V^{-1} for $W=3$ eV, and 0.72 V^{-1} for $W=1.5$ eV. Having a dc bias V_{stat} applied to the junction increases this responsivity. These values turn out to be of the same order as those obtained experimentally.[26,27] Higher classical responsivities can be achieved by *increasing* the gap spacing D. This, however, also increases the impedance R of the junction, which makes the coupling to a nanoantenna less efficient.

To illustrate the effects of a modification of the gap spacing D, we represented in Fig. 4 the diode impedance R achieved when considering a gap spacing D of 1.5 and 2.5 nm. The protrusion has the same radius r of 1 nm, so that the distance between the apex of the protrusion and the anode is 0.5 nm in the first case and 1.5 nm in the second. The classical responsivities achieved in these two situations are represented in Fig. 5. Reducing the gap spacing D from 2 to 1.5 nm decreases the impedance R of the junction to a value at zero bias of 3.3×10^4 Ω for $W=1.5$ eV. It, however, reduces the classical responsivities (maximal value of 1.5 V^{-1} for $W=1.5$ eV with $V_{\text{stat}}=1$ V). Increasing the gap spacing from 2 to 2.5 nm enhances the classical responsivities (maximal value of 6.6 V^{-1} achieved for $W=1.5$ eV). It, however, increases the diode impedance R (value at zero bias of $1.4\times10^9 V^{-1}$ for $W=1.5$ eV).

The rectified bias V_{rect} and the quantum efficiency $\eta_{\text{quant}}=[(\langle I\rangle-I_{\text{stat}})/(\langle P\rangle-V_{\text{stat}}I_{\text{stat}})]/[e/\hbar\Omega]$ of the rectification process are both proportional to the classical responsivity S. This responsivity appears in our results to increase with the gap spacing D. For applications related to the energy conver-

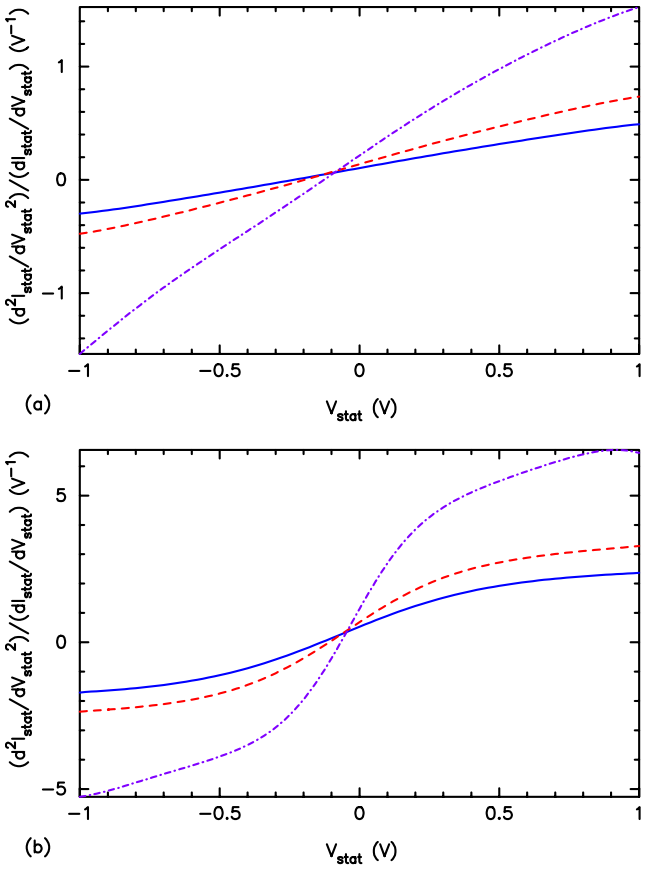

FIG. 5. (Color online) Classical responsivity $S=(d^2I_{stat}/dV_{stat}^2/dI_{stat}/dV_{stat})$ of a diode with gap spacings D of 1.5 nm (a) and 2.5 nm (b). The work functions W are 4.5 eV (solid), 3 eV (dashed), and 1.5 eV (dot-dashed). The height of the protrusion is 1 nm.

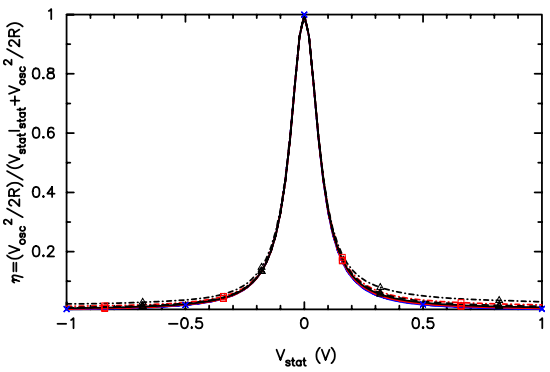

FIG. 6. (Color online) Conversion efficiency $\eta=(V_{osc}^2/2R)/[V_{stat}I_{stat}+(V_{osc}^2/2R)]$ for work functions W of 4.5 eV (solid), 3 eV (dashed), and 1.5 eV (dot-dashed). The three series of data correspond to gap spacings D of 1.5 nm (cross), 2 nm (square), and 2.5 nm (triangle). The height of the protrusion is 1 nm.

sion of incident radiations, the gap spacing D is in reality adjusted based on the matching condition between the coupled antenna and the tunneling junction and it is the energy converted per unit of time by the device that represents the quantity of interest. We established that $\langle P\rangle=V_{stat}I_{stat}+(V_{osc}^2/2)(dI_{stat}/dV_{stat})$, with $V_{stat}I_{stat}$ the power dissipated because of the application of V_{stat} and $(V_{osc}^2/2)(dI_{stat}/dV_{stat})=(V_{osc}^2/2R)$ the energy gained per unit of time from the source of the oscillating barrier. This last quantity is inversely proportional to the impedance R. Although the conversion process is less efficient for smaller gap spacings D, the impedance R will be smaller and the total energy converted from the source of the oscillating barrier will actually be more significant.

Considering that the dc power $V_{stat}I_{stat}$ is provided by the user and that $V_{osc}^2/2R$ is the power gained from the external radiation that provides V_{osc}, one can define a conversion efficiency $\eta=(V_{osc}^2/2R)/[V_{stat}I_{stat}+(V_{osc}^2/2R)]$ that is given by the ratio between the power $V_{osc}^2/2R$ gained from the source of the oscillating barrier and the total energy that circulates through the junction per unit of time (energy provided by the user plus energy gained from the source of the oscillating barrier). The results achieved for the three values of the gap spacing D (1.5, 2, and 2.5 nm) and the three values of the work function W (1.5, 3, and 4.5 eV), when considering an oscillating bias V_{osc} of 0.1 V, are represented in Fig. 6. These results are surprisingly similar. They indicate a value of $\eta=100\%$ when $V_{stat}=0$ V (there is in this case no input power from the user). The different curves turn out to decrease at the same rate. This can be understood by the fact that $I_{stat}\simeq V_{stat}/R(0)$, where $R(0)$ refers the impedance at zero bias. At small bias V_{stat} and considering the fact that R is maximum for $V_{stat}=0$ (vanishing first derivative), we actually have $R(V_{stat})\simeq R(0)$. The conversion efficiency therefore turns out to be well approximated by $\eta\simeq(V_{osc}^2/2)/[V_{stat}^2+(V_{osc}^2/2)]$, which is independent of any specific parameter but the amplitudes V_{stat} and V_{osc} of the voltage applied through the junction. We see that a conversion efficiency of $\eta=50\%$ is then achieved for $V_{stat}=V_{osc}/\sqrt{2}$, which determines the width of curves represented in Fig. 6. For energy-conversion applications in which the power $V_{stat}I_{stat}$ is provided by the user, this would represent the maximal bias V_{stat} to consider since the power gained from the radiation would be less than the energy supplied by the user if higher biases V_{stat} were considered.

We finally checked the influence of the aspect ratio of the protrusion on the impedance and classical responsivity of the junction. We thus increased the height of the protrusion from 1 nm to, respectively, 2 and 3 nm. We also increased the gap spacing D from 2 nm to, respectively, 3 and 4 nm in order to keep the distance between the apex of the protrusion and the anode to a value of 1 nm as in Fig. 1. We finally assumed that these protrusions have the same hemispherical termination as in Fig. 1 (radius of curvature r of 1 nm). These structures are represented in Fig. 7. It turns out that the impedance R and the classical responsivity S we obtain with these extended structures are essentially the same as those achieved when considering the structure in Fig. 1. This is illustrated in Fig. 8 where we represented the impedance R and the classical responsivity S achieved when considering a protrusion with heights of 1, 2, and 3 nm (with the same distance of 1 nm between the apex of these protrusions and the anode) and a work function W of 1.5 eV. This is essentially due to the fact the last 2 nm of region II are identical in

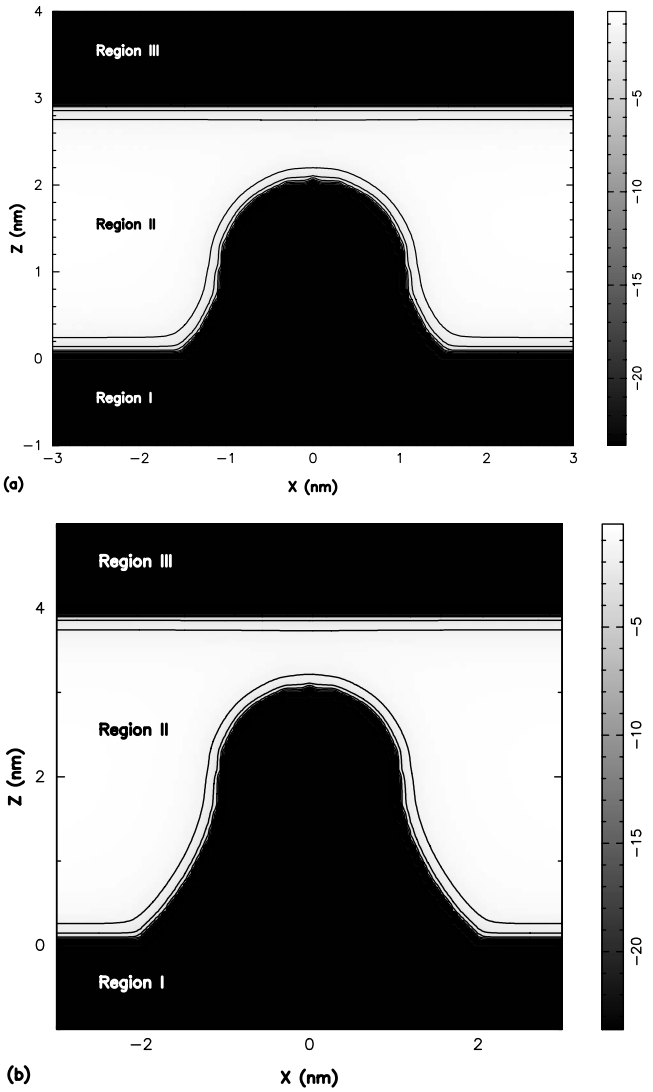

FIG. 7. Potential energy $V(\mathbf{r},t)$ in a metal-vacuum-metal junction. The representation corresponds to an external potential of 0 V. It includes the potential wells that characterize the metallic elements and the image potential in the vacuum. The heights of the protrusion are, respectively, 2 nm (a) and 3 nm (b). The gap spacings D are 3 nm (left) and 4 nm (right).

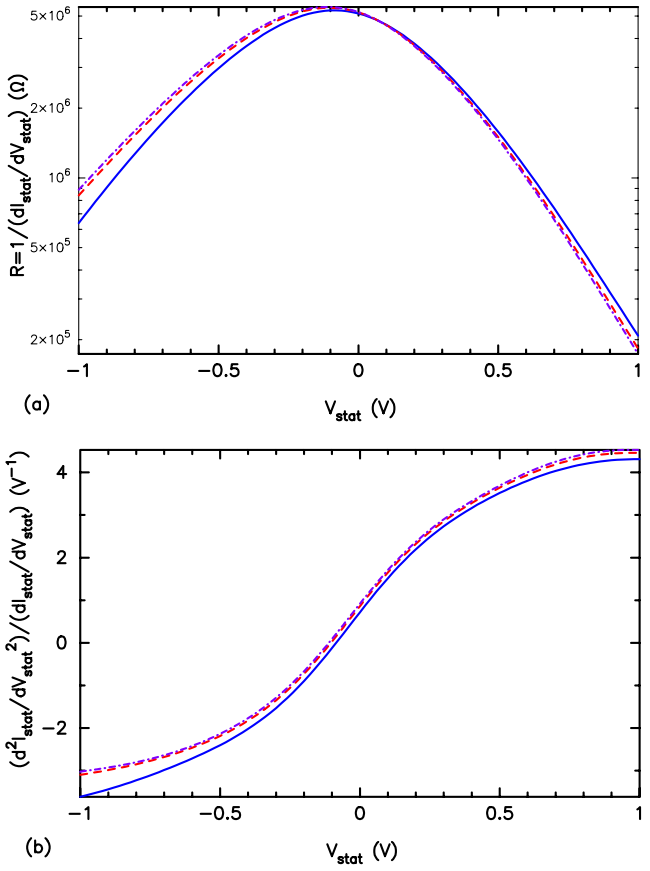

FIG. 8. (Color online) Impedance $R=1/(dI_{\text{stat}}/dV_{\text{stat}})$ (a) and classical responsivity $S=(d^2I_{\text{stat}}/dV_{\text{stat}}^2/dI_{\text{stat}}/dV_{\text{stat}})$ (b) of a diode whose protrusion has heights of 1 nm (solid), 2 nm (dashed), and 3 nm (dot-dashed). The anode is always at a distance of 1 nm from the apex. The work function is 1.5 eV.

the three cases. It shows that for the fundamental study of these metal-vacuum-metal junctions, it is appropriate to restrict these systems to the nanometer-size region in which the electronic tunneling processes actually take place. These simulations show that the work function of the materials and the distance between the apex of the protrusion and the anode are the important parameters to consider when studying these junctions.

V. DISCUSSION

The analysis presented in Sec. IV was based on the Taylor-expansion of static $I_{\text{stat}}(V_{\text{stat}})$ data and it was assumed that quantities of interest like $\langle I\rangle$ or $\langle P\rangle$ are represented with a sufficient degree of accuracy by an expansion limited to V_{osc}^2. It is interesting to consider at this point the results one would obtain by considering higher-order expansions of these quantities. It is also interesting to compare the results of this analysis with those one can obtain when the diode currents actually achieved with an oscillating barrier $V=V_{\text{stat}}+V_{\text{osc}}\cos(\Omega t)$ are computed exactly using the transfer-matrix technique.

The discussion will essentially focus on the classical responsivity. The classical responsivity S was introduced as a mean of calculating the rectified bias V_{rect}. This quantity was defined from $V_{\text{rect}}(dI_{\text{stat}}/dV_{\text{stat}})=\langle I\rangle-I_{\text{stat}}$ and we established that $V_{\text{rect}}=(\langle I\rangle-I_{\text{stat}}/dI_{\text{stat}}/dV_{\text{stat}})=(V_{\text{osc}}^2/4)S$, with $S=(d^2I_{\text{stat}}/dV_{\text{stat}}^2/dI_{\text{stat}}/dV_{\text{stat}})$ the classical responsivity. One can define an effective responsivity S_{eff} from the relation

$$S_{\text{eff}}=\frac{(\langle I\rangle-I_{\text{stat}})/(V_{\text{osc}}^2/4)}{dI_{\text{stat}}/dV_{\text{stat}}} \tag{6}$$

and compare the values achieved when using different approximations for the mean diode current $\langle I\rangle$. This effective responsivity still provides the rectified bias through $V_{\text{rect}}=(V_{\text{osc}}^2/4)S_{\text{eff}}$. It will, however, incorporate any correction factor that may improve the classical analysis presented in Sec. III.

We can thus compute the effective responsivity S_{eff} that corresponds to a mean diode current $\langle I\rangle$ given respectively by (i) $\langle I\rangle=I_{\text{stat}}+(V_{\text{osc}}^2/4)(d^2I_{\text{stat}}/dV_{\text{stat}}^2)$, (ii) $\langle I\rangle=I_{\text{stat}}$

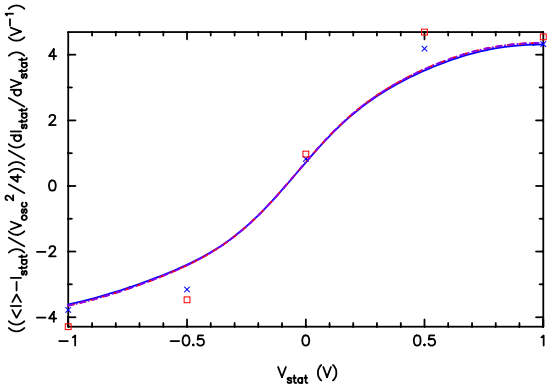

FIG. 9. (Color online) Effective responsivity $S_{\mathrm{eff}}=((\langle I\rangle - I_{\mathrm{stat}})/(V_{\mathrm{osc}}^2/4)/dI_{\mathrm{stat}}/dV_{\mathrm{stat}})$ achieved when computing $\langle I\rangle$ from $\langle I\rangle = I_{\mathrm{stat}} + (V_{\mathrm{osc}}^2/4)(d^2I_{\mathrm{stat}}/dV_{\mathrm{stat}}^2)$ (solid), $\langle I\rangle = I_{\mathrm{stat}} + (V_{\mathrm{osc}}^2/4)(d^2I_{\mathrm{stat}}/dV_{\mathrm{stat}}^2) + (V_{\mathrm{osc}}^4/64) \times (d^4I_{\mathrm{stat}}/dV_{\mathrm{stat}}^4)$ (dashed), $\langle I\rangle = I_{\mathrm{stat}} + (V_{\mathrm{osc}}^2/4)(d^2I_{\mathrm{stat}}/dV_{\mathrm{stat}}^2) + (V_{\mathrm{osc}}^4/64) \times (d^4I_{\mathrm{stat}}/dV_{\mathrm{stat}}^4) + (V_{\mathrm{osc}}^6/2304)(d^6I_{\mathrm{stat}}/dV_{\mathrm{stat}}^6)$ (dot-dashed), and the transfer-matrix technique for $\hbar\Omega=0.1$ eV (cross) and 0.2 eV (square). The gap spacing D is 2 nm. The height r of the protrusion is 1 nm. The work function W is 1.5 eV. The amplitude V_{osc} of the oscillating barrier is 0.1 V.

$+(V_{\mathrm{osc}}^2/4)(d^2I_{\mathrm{stat}}/dV_{\mathrm{stat}}^2)+(V_{\mathrm{osc}}^4/64)(d^4I_{\mathrm{stat}}/dV_{\mathrm{stat}}^4)$, (iii) $\langle I\rangle = I_{\mathrm{stat}}+(V_{\mathrm{osc}}^2/4)(d^2I_{\mathrm{stat}}/dV_{\mathrm{stat}}^2)+(V_{\mathrm{osc}}^4/64)(d^4I_{\mathrm{stat}}/dV_{\mathrm{stat}}^4) + (V_{\mathrm{osc}}^6/2304)(d^6I_{\mathrm{stat}}/dV_{\mathrm{stat}}^6)$, and (iv) a transfer-matrix calculation in which the time-dependence of the external bias $V = V_{\mathrm{stat}} + V_{\mathrm{osc}}\cos(\Omega t)$ is treated exactly. The system considered is that depicted in Fig. 1 (gap spacing D of 2 nm, height of the protrusion r of 1 nm and work function W of 1.5 eV). We used as previously $V_{\mathrm{osc}}=0.1$ V for the voltage induced by an external radiation. For comparison, Ward *et al.* inferred V_{osc} values around 30 mV from their measurements of laser-induced dc currents (radiation wavelength of 785 nm and power-flux density of 22.6 kW cm^{-2}).[28] From the work of Sullivan *et al.*,[48] we can expect in our case a junction biasing of 2 mV when considering solar radiation (this value is associated with an enhancement of the incident field amplitudes by a factor of 10^3 due to a receiving antenna). A beam focusing with an additional enhancement of the fields by a factor of 50 would therefore provide a biasing of 0.1 V. For the transfer-matrix calculations, we finally used $\hbar\Omega=0.1$ and 0.2 eV. These results are presented in Fig. 9. They show that the different Taylor expansions of $\langle I\rangle$ provide nearly identical results. An expansion of $\langle I\rangle$ to order V_{osc}^2 is thus sufficient for the system considered. The results provided by the transfer-matrix technique are comparable with the classical analysis in the limit when $\Omega\to 0$. Deviations however appear for finite frequencies. The mean diode current $\langle I\rangle$ actually achieved when the scattering problem is solved exactly is indeed higher than that predicted from the Taylor-expansion of static $I_{\mathrm{stat}}(V_{\mathrm{stat}})$ data. These deviations actually increase with Ω. This is essentially due to the fact electrons are promoted to higher energy levels because of the absorption of energy quanta $\hbar\Omega$. This process, which is not accounted for by the classical analysis of Sec. III, increases the tunneling probabilities and therefore the diode currents.[11] The effective responsivity S_{eff} achieved for $V_{\mathrm{stat}}=0$ V turns out to be 0.72 V^{-1} in the quasistatic limit where $\Omega\to 0$, 0.82 V^{-1} for $\hbar\Omega=0.1$ eV, 0.97 V^{-1} for $\hbar\Omega=0.2$ eV, 2.83 V^{-1} for $\hbar\Omega=0.5$ eV, 22.0 V^{-1} for $\hbar\Omega=1$ eV, and 35.8 V^{-1} for $\hbar\Omega=2$ eV.

A final point of discussion relates to the robustness of these calculations regarding possible variations in the electronic properties of the materials. The classical analysis technique presented in Sec. III relies on current-voltage data achieved in an idealistic static case ($\Omega=0$) in which the dielectric constant of the materials $\epsilon=-\infty$. This classical approach provides estimations for the current $\langle I\rangle$ and the power $\langle P\rangle$ achieved in the dynamic case ($\Omega\neq 0$) without, however, taking account of the frequency-dependence of ϵ. With tungsten, the effects of a variation of ϵ can be neglected for the range of frequencies considered (the plasma energy $\hbar\Omega_{\mathrm{p}}$ for tungsten is indeed as high as 22.8 eV).[33] For silver, there is a surface plasmon energy at 3.6 eV.[49] The variations in the dielectric constant must then be taken into account and the quantum-mechanical treatment presented in Sec. II will be more appropriate. As shown in Ref. 33, the occurrence of polarization resonances in the tip can increase dramatically the emission current $\langle I\rangle$ and thus the effective responsivity S_{eff}. In the case of a reduced screening of the external field (behavior expected for $\Omega\to\infty$), the effective biasing of the junction will decrease thus reducing the emission current $\langle I\rangle$ and the effective responsivity S_{eff}.

VI. CONCLUSIONS

We proposed a more detailed analysis of the rectification properties of geometrically asymmetric metal-vacuum-metal junctions. In order to establish results that can conveniently be compared with other experimental/theoretical work, we used a classical approach that is based on the Taylor-expansion of static current-voltage data. These static data were obtained using a transfer-matrix methodology for the consideration of quantum-mechanical effects and we compared in a final discussion the results of this classical approach with those obtained when solving the time-dependent scattering problem exactly. This work focused essentially on the impedance and classical responsivity of the junction. We showed that reducing the work function of the materials both reduces the junction impedance and enhances the diode responsivity, which constitutes the objective to achieve for the development of a device. Reducing the spacing between the cathode and the anode reduces the junction impedance. Increasing this spacing enhances the diode responsivity. It appears that a nanometer-size spacing between the apex of the emitter and the anode is a good compromise. It was shown that the main body of the protrusion has a smaller influence on the rectification process (the apex region in which the tunneling processes take place has a more significant impact). In conditions where the static bias V_{stat} is provided by the user and the oscillating bias $V_{\mathrm{osc}}\cos(\Omega t)$ is provided by an external radiation, one must respect $V_{\mathrm{stat}} < V_{\mathrm{osc}}/\sqrt{2}$ in order for the energy converted from this external radiation to be at least as important as the energy provided by the user (this conclusion turned out to apply to the different situations considered in this work). The classical responsivities defined

in this work are in good agreement with those achieved when considering higher-order expressions for the diode currents. Deviations, however, appear when the diode currents obtained with an oscillating barrier are computed using an exact quantum-mechanical scheme. Photon-absorption processes actually enhance the diode currents, which results in effective responsivities that are higher than those predicted from a classical analysis. The responsivities achieved at zero static bias for a work function of 1.5 eV and a distance of 1 nm between the apex of the emitter and the anode range from 0.72 V^{-1} in the infrared (classical result) up to 35.8 V^{-1} for a photon energy $\hbar\Omega$ of 2 eV in the visible. This comparison between classical and quantum-mechanical concepts will be explored with more details in future work. In its current form, this work already provides useful insight for the realization of a rectification device that may be used for the energy conversion of infrared and optical radiations.

ACKNOWLEDGMENTS

A.M. is funded as Research Associate by the National Fund for Scientific Research (FNRS) of Belgium. This work used resources of the Interuniversity Scientific Computing Facility located at the University of Namur, Belgium, which is supported by the F.R.S.-FNRS under Convention No. 2.4617.07. The authors acknowledge the support of the Paul H. Cutler Endowment Fund for Excellence of the Eberly College of Science, The Pennsylvania State University.

[1]T. E. Sullivan, P. H. Cutler, and A. A. Lucas, Surf. Sci. **54**, 561 (1976).
[2]K. H. Evenson, G. W. Day, J. S. Wells, and L. O. Mullen, Appl. Phys. Lett. **20**, 133 (1972).
[3]W. Krieger, T. Suzuki, M. Volcker, and H. Walther, Phys. Rev. B **41**, 10229 (1990).
[4]N. M. Miskovsky, S. H. Park, P. H. Cutler, and T. E. Sullivan, J. Vac. Sci. Technol. B **12**, 2148 (1994).
[5]C. Fumeaux, W. Herrmann, F. K. Kneubuhl, and H. Rothuizen, Infrared Phys. Technol. **39**, 123 (1998).
[6]N. Beverini, G. Carelli, E. Ciaramella, G. Contestabile, A. De Michele, and M. Presi, Laser Phys. **15**, 1334 (2005).
[7]T. E. Sullivan, Y. Kuk, and P. H. Cutler, IEEE Trans. Electron Devices **36**, 2659 (1989).
[8]A. A. Lucas, A. Moussiaux, M. Schmeits, and P. H. Cutler, Commun. Phys. (London) **2**, 169 (1977).
[9]N. M. Miskovsky, S. J. Shepherd, P. H. Cutler, T. E. Sullivan, and A. A. Lucas, Appl. Phys. Lett. **35**, 560 (1979).
[10]A. Mayer, M. S. Chung, B. L. Weiss, N. M. Miskovsky, and P. H. Cutler, Phys. Rev. B **77**, 085411 (2008).
[11]A. Mayer, M. S. Chung, B. L. Weiss, N. M. Miskovsky, and P. H. Cutler, Phys. Rev. B **78**, 205404 (2008).
[12]L. O. Hocker, D. R. Sokoloff, V. Daneu, A. Szoke, and A. Javan, Appl. Phys. Lett. **12**, 401 (1968).
[13]J. F. Mulligan, Am. J. Phys. **44**, 960 (1976).
[14]J. Terrien, Rep. Prog. Phys. **39**, 1067 (1976).
[15]K. M. Evenson, J. S. Well, F. R. Peterson, B. L. Danielson, G. W. Day, R. L. Barger, and J. L. Hall, Phys. Rev. Lett. **29**, 1346 (1972).
[16]Proceedings of the 17th General Conference on Measures and Weights, Sevres, France, 1983 (unpublished), p. 93.
[17]A. A. Lucas, P. H. Cutler, T. E. Feuchtwang, T. T. Tsong, T. E. Sullivan, Y. Yuk, H. Nguyen, and P. J. Silverman, J. Vac. Sci. Technol. A **6**, 461 (1988).
[18]H. Q. Nguyen, P. H. Cutler, T. E. Feuchtwang, Z.-H. Huang, Y. Kuk, P. J. Silverman, A. A. Lucas, and T. E. Sullivan, IEEE Trans. Electron Devices **36**, 2671 (1989).
[19]M. Tonouchi, Nat. Photonics **1**, 97 (2007).
[20]J. W. Schwede *et al.*, Nature Mater. **9**, 762 (2010).
[21]T. E. Hartman, J. Appl. Phys. **33**, 3427 (1962).
[22]K. B. Crozier, A. Sundaramurthy, G. S. Kino, and C. F. Quate, J. Appl. Phys. **94**, 4632 (2003).
[23]T.-D. Onuta, M. Waegele, C. C. DuFort, W. L. Schaich, and B. Dragnea, Nano Lett. **7**, 557 (2007).
[24]D. K. Kotter, S. D. Novack, W. D. Slafer, and P. J. Pinhero, ASME J. Sol. Energy Eng. **132**, 011014 (2010).
[25]P. Esfandiari *et al.*, Proc. SPIE **5783**, 470 (2005).
[26]P. C. D. Hobbs, R. B. Laibowitz, F. R. Libsch, N. C. LaBianca, and P. P. Chiniwalla, Opt. Express **15**, 16376 (2007).
[27]M. Dagenais, K. Choi, F. Yesilkoy, A. N. Chryssis, and M. C. Peckerar, Proc. SPIE **7605**, 76050E (2010).
[28]D. R. Ward, F. Huser, F. Pauly, J. C. Cuevas, and D. Natelson, Nat. Nanotechnol. **5**, 732 (2010).
[29]F. Yesilkoy, K. Choi, M. Dagenais, and M. Peckerar, Solid-State Electron. **54**, 1211 (2010).
[30]K. Choi, F. Yesilkoy, A. Chryssis, M. Dagenais, and M. Peckerar, IEEE Electron Device Lett. **31**, 809 (2010).
[31]J. R. Tucker, IEEE J. Quantum Electron. **15**, 1234 (1979).
[32]R. W. van der Heijden, J. H. M. Stoelinga, H. M. Swartjes, and P. Wyder, Solid State Commun. **39**, 133 (1981).
[33]A. Mayer and P. H. Cutler, J. Phys.: Condens. Matter **21**, 395304 (2009).
[34]A. Mayer, M. S. Chung, B. L. Weiss, N. M. Miskovsky, and P. H. Cutler, Nanotechnology **21**, 145204 (2010).
[35]A. Mayer and Ph. Lambin, Nanotechnology **16**, 2685 (2005).
[36]Th. Laloyaux, I. Derycke, J.-P. Vigneron, Ph. Lambin, and A. A. Lucas, Phys. Rev. B **47**, 7508 (1993).
[37]F. H. M. Faisal, *Theory of Multiphoton Processes* (Plenum, New York, 1987), pp. 8–10.
[38]A. Pimpale, S. Holloday, and R. J. Smith, J. Phys. A **24**, 3533 (1991).
[39]A. Mayer and J.-P. Vigneron, Phys. Rev. B **56**, 12599 (1997).
[40]A. Mayer and J.-P. Vigneron, Phys. Rev. E **59**, 4659 (1999).
[41]A. Mayer and J.-P. Vigneron, Phys. Rev. E **60**, 7533 (1999).
[42]A. Mayer and J.-P. Vigneron, Phys. Rev. E **61**, 5953 (2000).
[43]K. M. Evenson, *Quantum Metrology and Fundamental Physical Constants* (Plenum, New York, 1983), Vol. NATO ASI Series B-98, pp. 181–209.
[44]A. V. Bragas, S. M. Landi, and O. E. Martinez, Appl. Phys. Lett. **72**, 2075 (1998).
[45]R. Gupta and B. G. Willis, Appl. Phys. Lett. **90**, 253102 (2007).
[46]V. S. Fomenko, *Handbook of Thermionic Properties* (Plenum, New York, 1966), p. 20.
[47]K. R. Carver and J. W. Mink, IEEE Trans. Antennas Propag. **29**, 2 (1981).
[48]T. E. Sullivan, P. H. Cutler, and A. A. Lucas, Surf. Sci. **62**, 455 (1977).
[49]J. Daniels, C. Festenburg, H. Raether, and K. Zeppenfield, *Tracts in Modern Physics* (Springer, Berlin, 1970), Vol. 54, p. 77.